THE JOURNAL OF PHYSICAL CHEMISTRY C

pubs.acs.org/JPCC Article

Effect of SWCNT Content and Water Vapor Adsorption on the Electrical Properties of Cellulose Nanocrystal-Based Nanohybrids

Ainhoa Angulo Dehesa,[⊥] Francesca Luzi,[⊥] Debora Puglia, Erlantz Lizundia, Ilaria Armentano,* and Luigi Torre

Cite This: *J. Phys. Chem. C* 2020, 124, 14901−14910 Read Online

ACCESS | Metrics & More | Article Recommendations | Supporting Information

ABSTRACT: Cellulose nanocrystal (CNC)-based free-standing conductive films were prepared by introducing different contents of single-walled carbon nanotubes (SWCNTs) by an evaporation-induced self-assembly (EISA) process, using water as the sole solvent. The effect of SWCNT content on the morphology, thermal stability, and electric and dielectric properties of CNC films has been studied by field emission scanning electron microscopy (FE-SEM), thermogravimetric analysis (TGA), infrared spectroscopy (FT-IR), and X-ray diffraction (XRD). In order to investigate the effect of SWCNTs on the conduction mechanism of biobased nanohybrids, a detailed study on electrical and dielectric properties was conducted in DC and AC modes. The influence process parameters in terms of the dispersing agent and sonication method and the specific storage humidity conditions (RH = 0, 53, and 75%) were thoroughly investigated. The results arising from AC impedance spectroscopy were analyzed with respect to phase angle θ, the impedance imaginary part, and Nyquist plots, revealing the pivotal role of both SWCNT concentration and relative humidity in the electrical properties of nanohybrids. As a result, this work sheds light on the conducting mechanism of films based on cellulose nanoparticles in the presence of carbonaceous nanofillers.

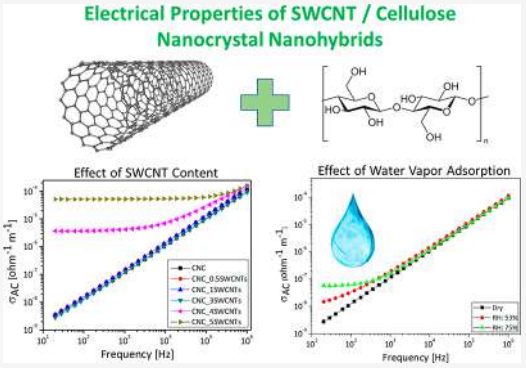

INTRODUCTION

Cellulose, as the most abundant renewable natural polymer on the biosphere, is being currently used for a large number of applications due to its excellent mechanical properties, chemical stability, biological compatibility, and remarkable hydrophilic properties.[1−3] Cellulose nanocrystals (CNCs) are a class of versatile nanosized materials based on cellulose that can be obtained from plants or bacteria. CNCs present a rod-like shape and dimensions typically ranging from 2 to 50 nm in width and 100 to 2000 nm in length.[4−6] The incorporation of CNC into more efficient multifunctional devices may lead to a significant advance in the next generation of eco-friendly materials. In this scenario, an important aspect is the possibility to develop free-standing, homogeneous films made of CNCs by using a water-based solvent evaporation process known as evaporation-induced self-assembly (EISA).[7] The dispersion of conductive nanostructures with a high aspect ratio in CNCs is a plausible approach to designing and synthesizing conductive and flexible paper-based multifunctional materials and devices,[8−10] with enhanced properties obtained by using different nanofiller contents. Among the available types of conductive nanofillers, single-walled carbon nanotubes (SWCNTs) are interesting candidates owing to their high aspect ratio and electrical conductivity.[11] The unique properties of SWCNTs arise from their 1D structure, according to their high length-to-diameter ratio which reduces the scattering of electrons,[12,13] with a honeycomb lattices of carbon atoms in sp^2 bonding. Their high aspect ratio allows electrical percolation at very low nanofiller loading, while the high intrinsic conductivity allows the production of systems with high bulk electrical conductivity. Therefore, the role of the SWCNTs within the CNC matrix would be to provide continuous conductive paths between different layers. So far, most of the studies have been focused on the development of new biobased materials with good electron-transfer capability, good stability, and a large surface area, which allow their use in different applications.[14]

The development of nanohybrid materials, which are composed of two or more components where CNCs act as a matrix and SWCNTs act as a conductive phase, has received increasing interest due to the synergistic properties originating from the nanosized components.[10,15] Combining the biobased properties and the large abundance in the nature of cellulose with the conductive nature of SWCNTs may allow an enlargement of the application field of the developed materials.

Received: April 16, 2020
Revised: June 6, 2020
Published: June 9, 2020

https://dx.doi.org/10.1021/acs.jpcc.0c03394
J. Phys. Chem. C 2020, 124, 14901−14910

Furthermore, incorporating conductive nanofillers within a nanocellulose matrix is an example of tailoring an approach of their characteristics for use in electronics and sensing devices, as well as studying the percolation threshold. Moreover, there is increasing interest in the development of CNC-based products for advanced technologies such as catalysis, batteries, supercapacitors, and sensing,[16−18] and how cellulose nanocrystals interact with the fluid interface is an important aspect in various fields.

In this sense, conductive nanohybrid films made from CNCs were explored as humidity sensors,[18] and due to the many hydrophilic functional groups in the material (hydroxyl, ether, carboxyl, and carbonyl of the graphene oxide), the material provided a fast and linear capacitance change (on the log scale) within the relative humidity range of 25 to 90%. Overall, the obtained good sensitivities and repeatability together with the cost-effective character of developed materials make CNC-based hybrids good candidates for developing low-power-consumption and environmentally safer sensing devices.

With this in mind, the aim of this study was to develop conductive nanohybrids based on CNCs and SWCNTs and investigate the electrical and dielectrical properties of the developed nanohybrid materials as a function of SWCNT content. Furthermore, the effect of the relative humidity conditions was explored because the electrical properties of cellulose are greatly influenced by the adsorption of water vapor. In this work, the dielectric relaxation spectroscopy was also utilized to understand the conduction mechanism and the microstructure of the nanohybrid films.

EXPERIMENTAL SECTION

Materials. Single-walled carbon nanotubes (SWCNTs) were supplied by Thomas Swan & Co. Ltd. (Elicarb, Durham, U.K.), with typical nanotube dimensions of 2 nm in diameter and ca. 1 μm in length, and were used as received.

Microcrystalline cellulose with a particle size of 20 μm, sulfuric acid (H_2SO_4), sodium dodecyl sulfate (minimum 98.5%, GC), silica gel (SiO_2), magnesium nitrate-6-hydrate ($Mg(NO_3)_2$, sodium chloride (NaCl), and sodium dodecyl sulfate (SDS) were purchased from Sigma-Aldrich and used as received.

Cellulose nanocrystals (CNCs) were synthesized via the sulfuric acid hydrolysis of microcrystalline cellulose.[7,19] Microcrystalline cellulose was hydrolyzed in a 64 (w/w)% sulfuric acid solution at 45 °C for 30 min. The reaction was quenched by adding 20-fold distilled water. The remaining cellulose was recovered by centrifugation (4100 rpm for 20 min), and it was further dialyzed for 7 days using a dialysis tubing cellulose membrane (Sigma-Aldrich). Then, a mixed-bed ion-exchange resin (Dowex Marathon MR-3 hydrogen and hydroxide forms) was added for 24 h. After vacuum filtration, a CNC aqueous suspension was obtained.

Nanohybrid Film Processing. SWCNT-loaded CNC nanohybrid films were fabricated by evaporation-induced self-assembly (EISA). The required amounts of SWCNTs were finely dispersed in distilled water (in a 1 mg/1 mL concentration) via tip sonication (30% output for 30 min; Vibra-CellTM CV 334), and they were added to aqueous CNC (2 wt %) dispersions to obtain 0.5, 1, 3, 4, and 5 wt % solutions (SWCNT concentration in CNC). Then, another sonication step (5 min and 20% output Vibra-CellTM CV 334) and a stirring step (30 min, in the case of 3, 4, and 5 wt % films, at ∼100 °C were used to evaporate the excess of water) were applied to dispersions before casting them onto Teflon dishes. Due to the poor dispersion in the films with 4 and 5 wt % SWCNTs, the stirring step was replaced by bath sonication (50 min, 40% of the amplitude at ∼60 °C). Bath sonication was also considered in the case of high SWCNT content. The use of a surfactant was also considered with the aim of improving the dispersion; therefore, an aqueous solution of sodium dodecyl sulfate (SDS) at 1 wt % was added to the SWCNTs.

Nanohybrid Film Characterization. The morphology of CNC-based films was investigated using a Hitachi S-4800 field emission scanning electron microscopy (FE-SEM) instrument at an acceleration voltage of 5 kV. Before characterization, cryogenically fracture surfaces were gold-coated with a 10-nm-thick layer using an Emitech K550X sputter coater.

Thermogravimetric analysis (TGA) was performed on 10 mg samples with a Seiko Exstar 6300 TGA quartz rod microbalance. The tests were conducted under a nitrogen atmosphere from 100 to 600 °C at 10 °C/min.

Fourier transform infrared spectroscopy (FT-IR) analysis of CNCs and CNC_SWCNTs nanohybrid films was performed at room temperatures in reflection mode by attenuated total reflectance (ATR) using a Jasco FT-IR 615 spectrometer with 4 cm^{-1} spectral resolution. The measurements were performed on CNC powder, a CNC film, and CNC_SWCNT films.

Room-temperature X-ray powder diffraction (XRD) patterns were obtained on a Bruker D8 Advance diffractometer equipped with a Cu tube, a Ge(111) incident beam monochromator (λ = 1.5406 Å) (fixed slit 1 mm), and a Sol-X energy-dispersive detector (fixed slit 0.06 mm). Samples were mounted onto a zero background silicon wafer embedded in a generic sample holder.

Bulk electrical resistivity measurements were conducted (ASTM D-257) by using a Keithley 6517A electrometer by applying a square wave ranging from 25 V (for pure CNC) to 0.1 V (for percolated nanohybrids) with a period of 120 s for at least four measurements for each sample.

The real and imaginary parts of the complex impedance (Z^*) of the CNC and CNC-based SWCNT films were analyzed with a Hewlett-Packard 4284A Precision LCR Meter in the 20 Hz−1 MHz frequency range. The specific AC conductivity of the samples as a function of frequency $\sigma(\omega)$ is calculated as reported in eq 1

$$\sigma_{AC} = d/(|Z|A) \quad (1)$$

where A is the cross-sectional area and d is the sample thickness, which is measured with a Borletti MELN/1W micrometer (0−25 Mm).

Since CNCs are very sensitive to humidity, films were kept in desiccators with different saturated salts for several days before each measurement in order to stabilize them at a given relative humidity (RH). Mass variation of the film was measured at different times. A stable condition was achieved after at least 1 day of storage. The following compounds were used: silica gel (SiO_2, RH = 0%), magnesium nitrate-6-hydrate over saturated solution, $Mg(NO_3)_2$(RH = 53%), and sodium chloride NaCl (RH = 75%).

RESULTS AND DISCUSSION

Microstructure. The microstructure of the prepared nanohybrid films was first investigated by FE-SEM. Micrographs, showing the fracture cross sections of CNC_SWCNT films in Figure 1, reveal the formation of dense materials with

https://dx.doi.org/10.1021/acs.jpcc.0c03394
J. Phys. Chem. C 2020, 124, 14901−14910

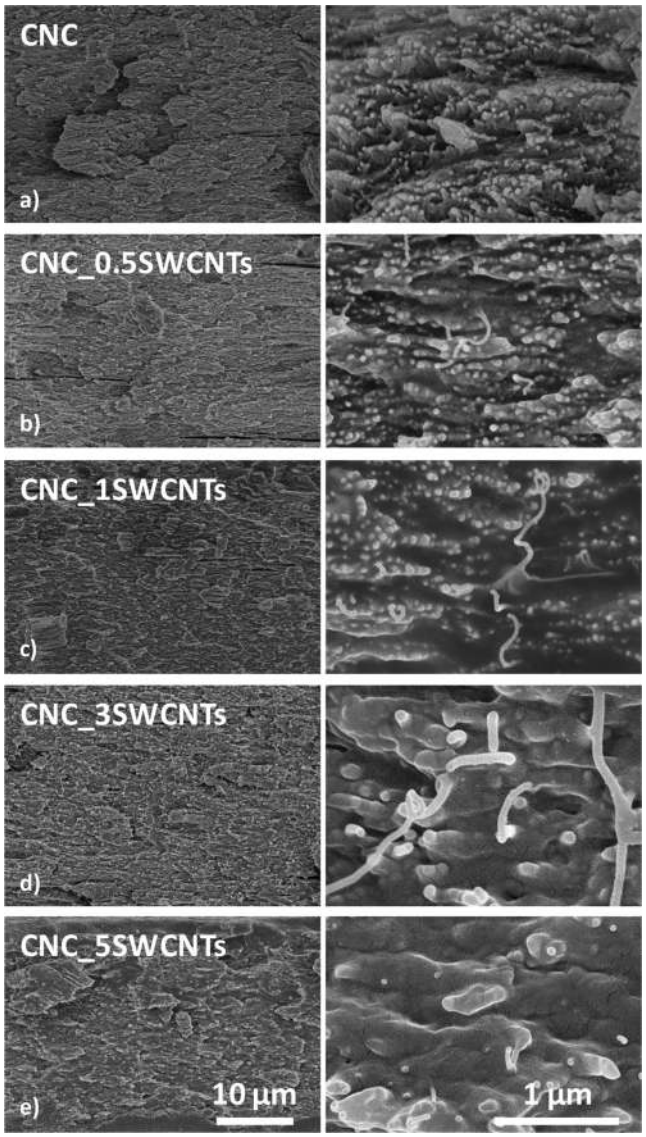

Figure 1. FE-SEM images viewed along fracture cross sections of CNC_SWCNT nanohybrid films for different SWCNT concentrations at two different magnifications.

no voids for all of the compositions. CNCs form a closely packed structure in which SWCNTs remain homogeneously dispersed. (See Figure S1 for a detailed view of the SWCNT distribution within the cellulosic matrix.) During the dispersion of CNCs with SWCNTs in water, the long-range electrostatic repulsion forces between negatively charged CNCs can keep carbon nanotubes well-dispersed in the solution, allowing the nanohybrid constituents to remain dispersed in water without aggregation and further precipitation (indeed, several works have used CNC as dispersing agents for SWCNTs).[20,21] Upon solvent drying and subsequent coassembly of CNC with SWCNTs through EISA, this favorable dispersion state can be kept to yield solid films with well-dispersed conducting nanotubes.[22,23]

After the evaporation of the dispersing media, CNC and SWCNTs cannot remain separated, yielding to the formation of irreversible intermolecular hydrogen bonds between adjacent CNCs, van der Waals forces between nanotubes, and cation−π interactions.[24] As a result, the above-mentioned dense structure is achieved.[25,26]

It can be observed that nanohybrid films present SWCNTs out of the fracture plane, suggesting that upon surface fracture, besides the CNC hydrogen bond breakage, carbon nanotubes need to be pulled out. Accordingly, direct evidence for the SWCNT reinforcement is shown here. In any case, concentrations larger than 4 wt % also yield aggregated SWCNT bundles (diameters up to 3 μm) due to the van der Waals forces between neighboring nanotubes (Figure S2).

The effect of the processing conditions on the morphology of resulting films is shown in Figure 2. Small differences are observed upon SDS incorporation into CNC films (left column (CNC vs CNC + SDS) and middle column (CNC_1SWCNTs vs CNC_1SWCNTs_SDS)).

FE-SEM images of CNC films produced by adding SDS surfactant with and without SWCNTs are reported, revealing a rougher surface structure with a packed CNC microstructure in the absence of SDS. The introduction of SDS leads to smoother and more homogeneous films. In the case of surfactant-stabilized SWCNTs and CNC, we expect that SDS remains distributed at the interface of the nanotubes and CNC, improving the nanometer dispersion by wrapping on the surface of the SWCNTs.[27]

Additionally, as depicted in the images shown in the right column of Figure 2, bath sonication does not induce any relevant visible morphological change in the resulting film.

Thermogravimetric Analysis. Figure 3a,b shows thermogravimetric (TG) and derivative thermogravimetric (DTG)

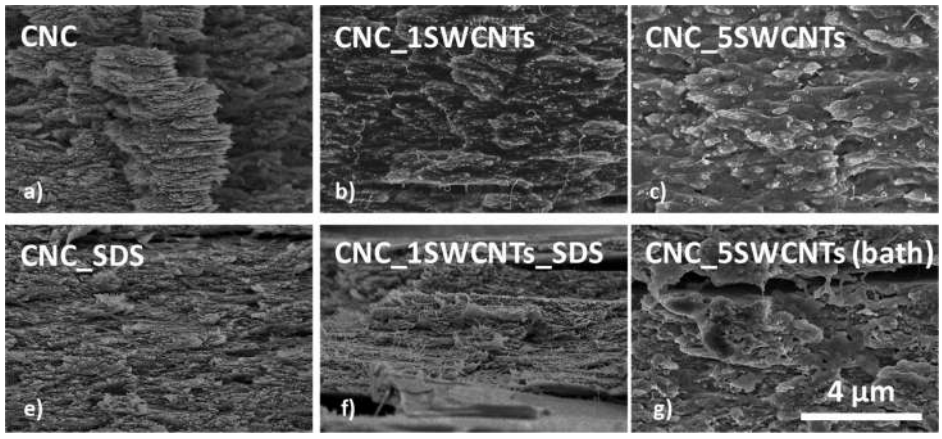

Figure 2. FE-SEM images viewed along fracture cross sections of CNC_SWCNT nanohybrid films obtained through different processing methods.

https://dx.doi.org/10.1021/acs.jpcc.0c03394
J. Phys. Chem. C 2020, 124, 14901−14910

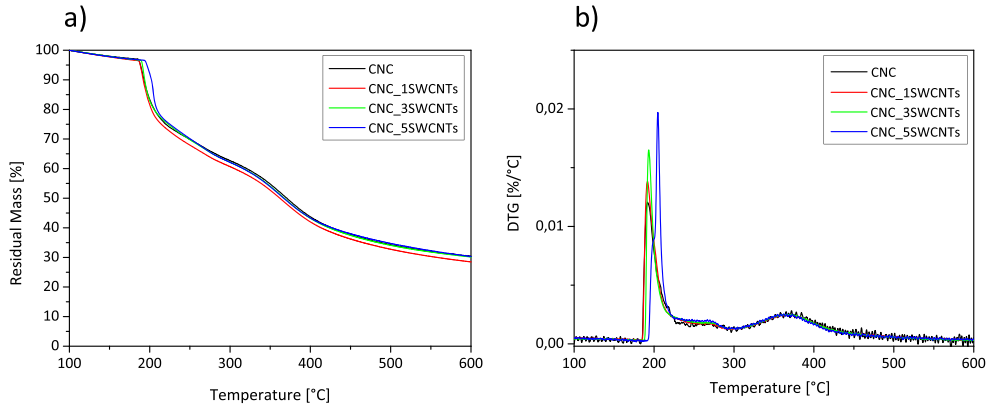

Figure 3. (a) TG and (b) DTG curves of CNC_SWCNT nanohybrid films for different SWCNT concentrations.

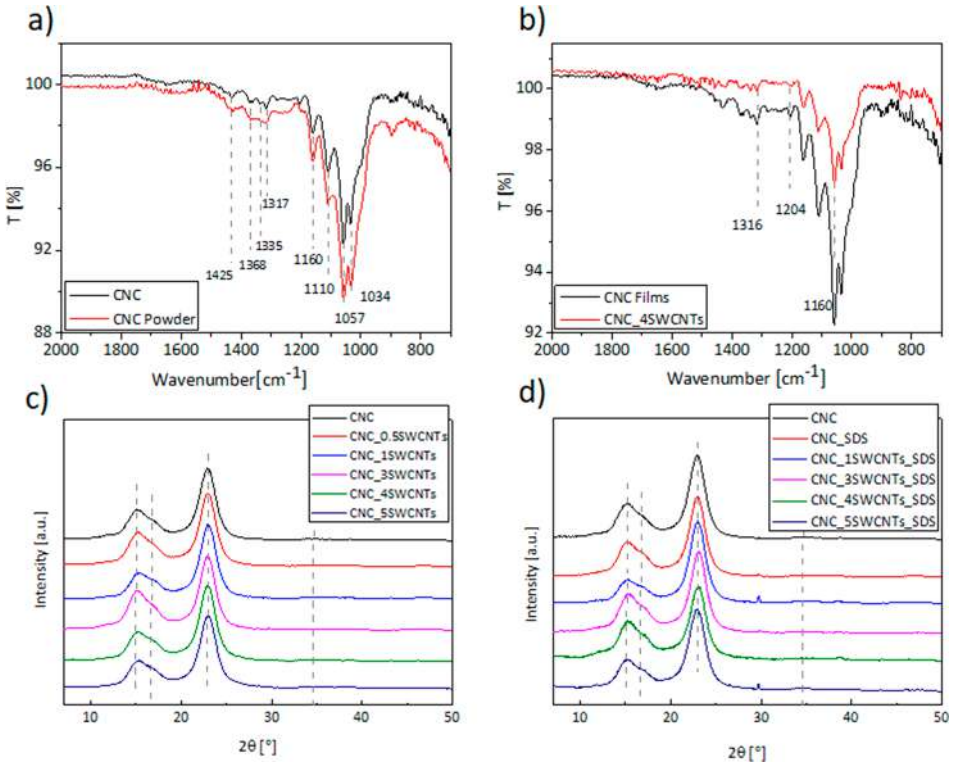

Figure 4. FT-IR spectra of (a) CNC films and powder and (b) CNC and CNC_4SWCNTs films. Room-temperature XRD patterns of prepared composite films: (c) effect of SWCNT concentration and (d) effect of SDS.

curves of CNC_SWCNT nanohybrid films, representative of weight losses and degradation rates during heating in a nitrogen atmosphere, respectively. A neat CNC film begins to degrade at 185 °C and reaches its maximum degradation rate at 192 °C (T_{peak}) with a maximum degradation rate (DTG_{max}) at this temperature of 0.012%/°C, due to the depolymerization, dehydration, and decomposition of cellulose glycosyl units induced by the temperature increase.[19] CNCs exhibited their main weight loss in the temperature range of 250−400 °C, at which the depolymerization of cellulose occurs along with dehydration and decomposition to produce char and volatile products,[28,29] while the third mass loss can be related to the degradation of sulfated ends of crystalline regions, which is visible in the case of highly sulfated samples.[30]

While no substantial variation was noted with the addition of 1 wt % SWCNTs, the thermodegradation process of nanohybrids was continuously delayed upon the addition of SWCNTs with an increase in DTG_{max} values and a shift of the thermal degradation events at 182 and 192 °C, respectively, for CNC_3SWCNTs and CNC_5SWCNTs. The two-stage thermodegradation process occurring in CNC films was confirmed even at the high content for SWCNTs. A slightly different DTG profile below 240 °C was noted in the case of CNC_5SWCNTs, where a shoulder appeared at 198 °C, due to the catalytic effect imposed by the presence of carbon-based nanoparticles.[31,32]

Physicochemical Conformation and Crystalline Structure. The analysis of FT-IR spectra of CNC (in powder and film) (Figure 4a,b) revealed the presence of easily identifiable peaks for cellulose (peak at 1649−1634 cm^{-1}, due to O−H bending of adsorbed water, CH_2 wagging at 1317 cm^{-1}, C−C ring stretching at 1160 cm^{-1} and peaks for C−O−C glycosidic ether, C−O−C pyranose ring stretching, and γCO at C−6 found at 1110, 1057, and 1034 cm^{-1}, respectively.[33] EISA film

https://dx.doi.org/10.1021/acs.jpcc.0c03394
J. Phys. Chem. C 2020, 124, 14901−14910

processing does not affect the CNC chemical structure. Shifts in the peaks located at 1425 cm^{-1} (O−C−H and CH_2 scissoring), 1368 cm^{-1} (CH bending), and 1335 cm^{-1} (OH in-plane bending) were observed after film processing in the spectrum of the CNC. The addition of the SWCNTs did not change the positions of the identified peaks, and no new peaks were found. Only a few variations in the intensities at 1316, 1204, and 1160 cm^{-1}, corresponding respectively to C−H bonding and C−C ring stretching, were noted.[34]

Figure 4c shows the X-ray diffraction (XRD) patterns of prepared nanohybrids films. The diffraction pattern of all of the samples is dominated by three main peaks centered at 2θ angles of 14.9, 16.5, and 22.7°, which are identified as the ($\bar{1}10$), (101), and (200) planes of the cellulose I form.[35,36] An additional weak peak corresponding to the (004) plane of cellulose I is also observed at 2θ = 34.4°. As depicted in Figure 4c, no additional peaks are observed upon SWCNT incorporation. In this sense, it has been reported that SWCNTs display a broad main diffraction peak at a 2θ angle of 26.6 ascribed to the (002) plane of hexagonal graphitic carbon.[37] The absence of the peak corresponding to SWCNTs is related to the small fraction of SWCNTs within the composite film, whose diffraction pattern is dominated by the highly crystalline CNC (degree of crystallinity, $X_c \approx 91\%$ according to Ruland's principles and Rietveld analysis).[34]

Similarly, Figure 4d shows the effect of SDS addition and batch processing on the crystalline structure of resulting materials. SDS incorporation yields new narrow diffraction peaks which match the monoclinic lattice of SDS ($P21/c$ space group) reported by Smith et al.,[38] suggesting that homogeneously distributed small crystals are formed between CNCs.[39] Moreover, the main broad peaks corresponding to the CNC matrix remain unchanged. Furthermore, it is seen that after bath sonication the XRD pattern of the CNC_5SWCNTs film remains virtually unchanged. Overall, the fact that CNC diffraction peaks do not change their shape or position is due to the fact that their crystalline structure is defined during the sulfuric acid hydrolysis and remains stable upon film formation.

Electrical and Dielectrical Properties. Figure 5 shows the DC conductivity (σ_{DC}) of the CNC_SWCNT nanohybrid EISA films in the log plot, as a function of the SWCNT content in the 0.5−5 wt % range, in dry form. The σ_{DC} increases with the increase in the SWCNT loading, as already observed in the case of other SWCNT-based nanohybrids.[40] With a single-walled carbon nanotube content of less than 3 wt %, the conductivity was below the value of 10^{-10} Ω^{-1} m^{-1}, and the films maintain the insulating properties of the original neat CNC films. Nanohybrids with 4 and 5 wt % SWCNTs show an increase in the conductivity of 5 orders of magnitude with values higher than 10^{-6} Ω^{-1} m^{-1} due to SWCNT conductive network formation.

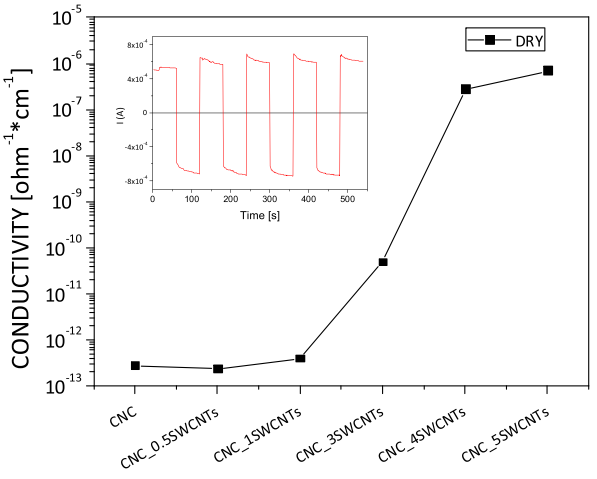

Figure 5. DC conductivity as a function of SWCNT content in cellulose-nanocrystal-based films. The inset shows the behavior of the current of CNC_5SWCNTs as a function of the time when a square wave of 1 V is applied.

The inset of Figure 5 shows the typical behavior of the current for CNC_5SWCNTs films as a function of time, when a square wave of 1 V was applied. Over a wide range of voltage, there is a linear correlation between the current and voltage, indicating that ohmic contacts between nanohybrid films and electrodes are formed.

Dielectric spectroscopy was used in this study to analyze the frequency-dependent electrical properties of the SWCNT-based films under dry and a fixed-humidity conditions[41] since it represents a valuable tool for studying the relationships between the electrical properties of the nanohybrids and their internal microstructure. The real and imaginary parts of the impedance are recorded under different humidity conditions. Stable humidity conditions were assured after 24 h of incubation. The addition of a conductive phase as SWCNTs in a CNC natural polymer matrix promotes the conductive behavior, as already demonstrated by the DC study in Figure 5.

The data were analyzed in terms of AC conductivity (σ_{AC}), phase angle θ, and real and imaginary parts of the impedance.[42]

Figure 6a−c shows the σ_{AC} conductivity behavior of the CNC-based films for various SWCNT contents and measured under (a) dry conditions, (b) 53% relative humidity (RH), and (c) 75% RH. The frequency dependence of conductivity shows two distinct regimes: (i) the low-frequency plateau region and (ii) the high-frequency dispersion region. The plateau region corresponds to frequency-independent conductivity (σ_{DC}), and the dispersion region corresponds to the frequency-dependent part. The σ_{AC} of the pure CNC film increases almost linearly with increasing frequency, showing typical insulating behavior. This effect was also observed in nanohybrids with SWCNT content of less than 3 wt %. When the content is higher than 3 wt %, the nanohybrids exhibit metal-like conductive behavior, and their σ_{AC} becomes frequency-independent at low frequencies to increase later with the frequency. These results indicate that carbonaceous nanostructured networks are formed. A critical frequency (f_c), which is function of the SWCNT content in the films and of the environmental conditions, can be defined as the level where the σ_{AC} curve became independent of the frequency. In our study, we can observe that in the dry state the 3 wt %-based film exhibit insulator behavior, while at 53% RH σ_{AC} of the same sample shows a critical frequency at around 100 Hz, which increases up to 1000 Hz for the sample being tested at 75% RH. In the case of 5 wt % SWCNTs, this value increases up to 10 000 Hz. It is well established that the conductivity and the impedance of materials depend upon the orientation of the permanent dipoles.[43] The dipoles can be oriented by the change in the content of the conductive phase as SWCNTs but also by changing the surrounding humidity, hence the water adsorption in the CNC, that can affect the mobility of bound charges.

In Figure 6d−f, for phase angle θ, the out-of-phase behavior between current and voltage ($\arctan(Z_i/Z_r)$) is plotted against

https://dx.doi.org/10.1021/acs.jpcc.0c03394
J. Phys. Chem. C 2020, 124, 14901−14910

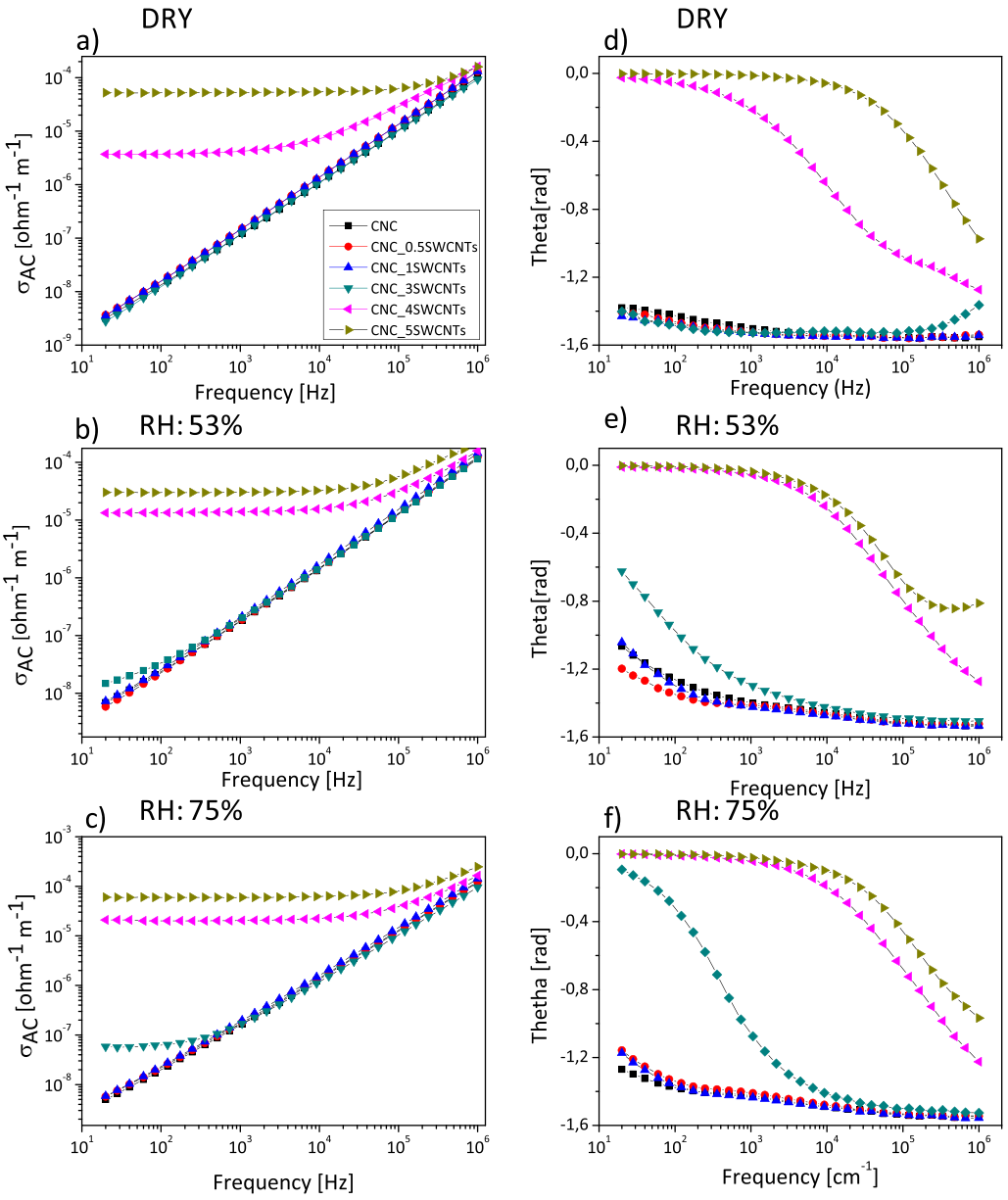

Figure 6. Role of the SWCNT content in the AC conductivity and phase θ angle behavior in the 20 Hz −1 MHz frequency range, measured (a−d) under dry conditions, (b−e) at a relative humidity fixed at 53%, and (c−f) at a relative humidity fixed at 75%.

frequency. From phase angle values, it is possible to observe that a high SWCNT content is related to a material with a θ value close to zero rad, in the low-frequency region, which can be associated with more resistive-like behavior. Due to the conductive nature of nanotubes, the material loses its dielectric nature. On the other hand, lower SWCNT content (i.e., 3 wt %) leads to a θ value of about −1.4 rad, which can be related to more capacitive-like behavior. Moreover, these curves confirm that the conductive nature is predominant at low frequencies, while at higher frequencies the capacitive behavior provides a constant value for the phase curve. A relaxation phenomenon is visible in the CNC_SWCNTs EISA films with SWCNT content below 3 wt %, and this effect is RH%-dependent. Furthermore, CNC films without conductive nanofillers show changes induced by the different relative humidity conditions, with a difference in the relaxation of charged mobile species, within the range of the studied frequencies.[44] Dielectric spectroscopy is highly sensitive to charge mobility and the local dynamics of dipole moments that can be changed by water interaction with CNC. The transport mechanism induced by carrier ions (protons and/or cations) may explain the observed changes in the phase angle θ in conductivity with moisture content.

The relative humidity conditions also have a strong influence on the electrical and dielectric properties of the nanohybrids. Figure 7 shows in detail the trends in (a) AC conductivity, (b) phase angle θ, (c) the imaginary part of the impedance, and (d) the Nyquist plot of CNC_3SWCNTs under different relative humidity conditions, while the behavior of the sample CNC_4SWCNTs film is reported in Figure S3.

It is well known that CNCs, as all polysaccharides, can strongly interact with water molecules.[45] Here, the conductivity was measured for films stabilized at various relative humidities. As shown in Figure 7a, the AC conductivity decreases when the films are dried, forming an insulating structure at low relative humidity. Conversely, an increase in

https://dx.doi.org/10.1021/acs.jpcc.0c03394
J. Phys. Chem. C 2020, 124, 14901−14910

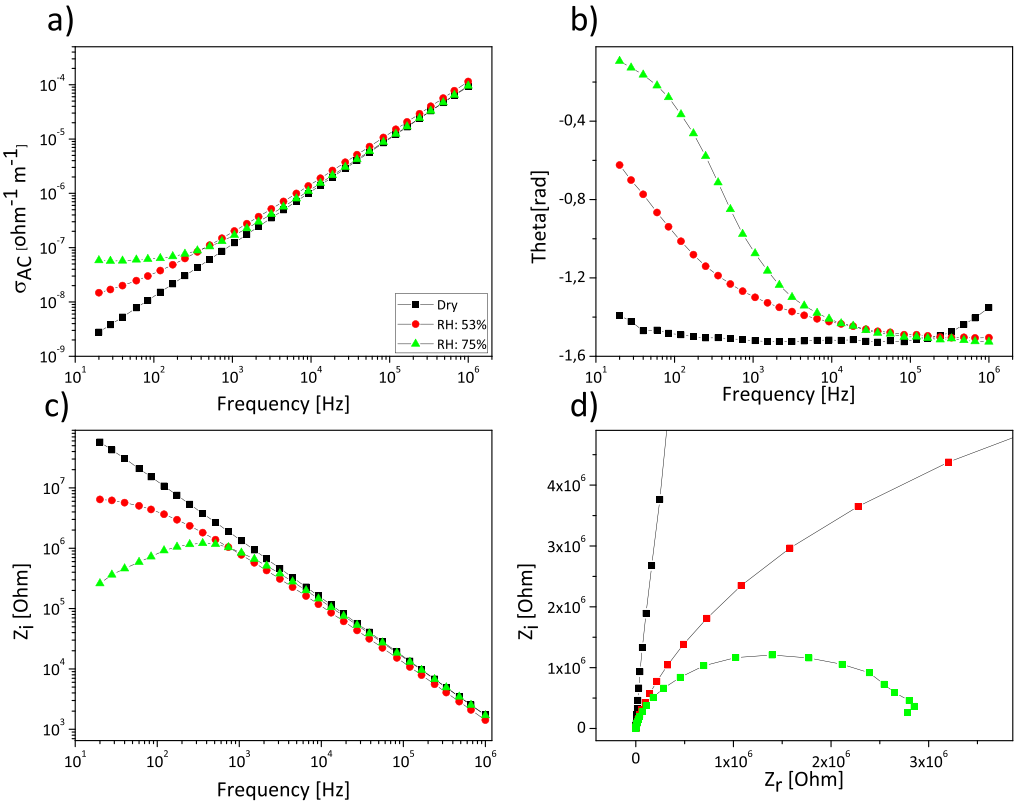

Figure 7. (a) AC conductivity, (b) phase angle θ, (c) imaginary part of Z versus frequency, and (d) a Nyquist plot for CNC_3SWCNTs EISA films stabilized at various RH values.

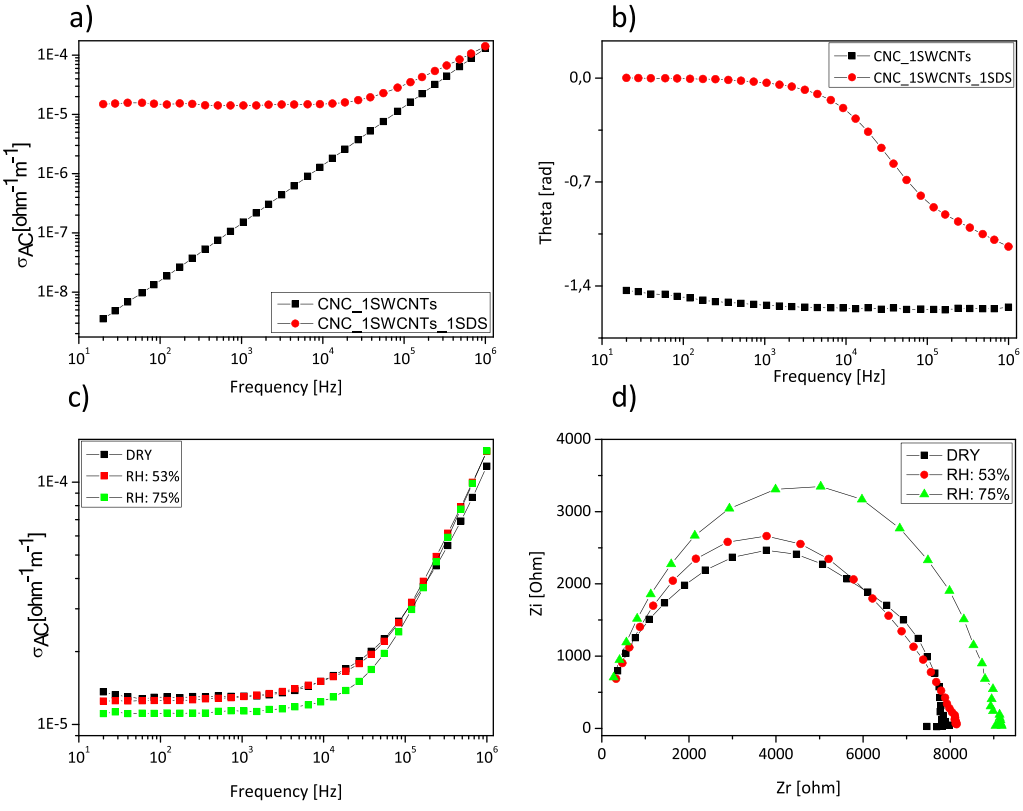

Figure 8. Role of SDS in CNC_1SWCNTs films: (a) AC conductivity and (b) phase angle θ versus frequency in the dry state. (c) AC conductivity versus frequency and (d) Nyquist plot for CNC_1SWCNTs _SDS EISA films stabilized at various RH values.

https://dx.doi.org/10.1021/acs.jpcc.0c03394
J. Phys. Chem. C 2020, 124, 14901−14910

the relative humidity is accompanied by an enhancement in the conductivity. Water may act as a plasticizer in the amorphous segments and tends to build a large number of inter-CNC hydrogen bonds between the hydroxyl groups, reinforcing lateral cohesion. This leads to a better organized and denser network with rubbery characteristics at high moisture contents rather than a rigid network at low moisture contents.[46] Figure 7b represents the frequency dependence of the phase-shift angle. In our obtained nanohybrids, the shifts from negative to positive on the CNC_3SWCNTs film increase with the relative humidity, indicating the occurrence of a capacitive-inductive transition, induced by the presence of adsorbed water molecules. The observed θ behavior means that the voltage phase falls behind the current phase and capacitors play a dominant role in the circuit, so the nanohybrids manifest capacitive character. CNC_3SWCNTs films exhibit insulator behavior in the dry state.

The log−log plot of the imaginary part of the impedance (Z_i) (Figure 7c) exhibits linear behavior with the frequency, whereas when the measurements were conducted on stabilized films at 53 and 75% RH, a peak was observed corresponding to the relaxation of charged mobile species, within the range of the studied frequencies, which was shifted toward higher frequency with increasing RH.[44] To better understand the complex dielectric behavior of the studied samples, the Nyquist plot, representative of Z'' versus Z' on a normal scale plot, is displayed in Figure 7d as a function of storage humidity conditions. It exhibited a semicircle shape, indicating the presence of polarization with a single relaxation time.[47] The peak and radius of the semicircle decrease with the increase in humidity but also with the SWCNT content. Similar behavior was observed in the case of CNC_4SWCNTs nanohybrid films (Figure S3), where the frequency shift in the relaxation peak of the imaginary part of the impedance is very visibile and attributed to the water adsorption.

SDS was used as a dispersing agent in SWCNT-based nanohybrid films since the dispersion of carbon nanotubes and their mixing with nanocellulose on the nanometric scale is one of the most difficult challenges for creating conductive films. SDS is usually distributed at the interface of the nanotubes but is also present in the bulk polymer matrix.[27,48] Dielectrical analysis shows how the presence and the dispersion action induced by the SDS improve the electrical transport network. Increased values of conductivity (Figure 8a) were obtained in SDS-based films by comparison with the same film formulation without SDS and measured under the same laboratory conditions. Phase angle θ (Figure 8b) also exhibits more resistive-like behavior. This result is speculated to be the competition between the increased dispersion of nanotubes and the deterioration of SWCNT electrical conductivity by SDS adsorption. Dielectric spectroscopy shows that SDS induces the formation of a relaxation mechanism, underlining that interfacial phenomena induced by the presence of SDS are critical.

The role of the SDS dispersion agent in carbon nanotubes was also analyzed under different relative humidity conditions. Figure 8c,d compares the AC conductivity versus frequency and the Nyquist plot for CNC_1SWCNTs_SDS films stabilized at various RH values. The films exhibit very similar behavior, without showing a large difference for the dry state, at 53 and 75% RH, in SWCNT-based films with the SDS dispersing agent. It seems that water interacts in a different manner with the SDS-based CNC_SWCNTs films. When the dispersion state of SWCNTs is poor and they are agglomerated in the cellulose nanocrystals, the system can absorb a considerable amount of water, which modifies the electrical properties.

SDS is a typical head-and-tail surfactant, which is composed of a hydrophobic tail and a polar headgroup. SDS molecules can induce a well-organized molecular structure, as shown by Tan et al.,[49] on the surface of the SWCNTs due to the interchain van der Waals interaction between the alkyl chains. However, the ionic sulfate group is expected to interact with the CNC surface, whereas the hydrophobic alkyl chains adsorb on the SWCNTs. The final structure depends on the interactions among the following: SDS, CNCs, and SWCNTs.[50]

CONCLUSIONS

This work presents a green method for the fabrication of electrically conductive CNC-based nanohybrids by dispersing SWCNTs and by using water as a unique solvent. The effects of the SWCNT content and dispersing agent were mainly investigated. Chemical, thermal, and morphological analyses underlined that SWCNTs are well dispersed in the CNC films. The results demonstrate the importance of analyzing both the DC conductivity and the dielectric properties in order to obtain in-depth information about charge-transport phenomena. The results presented in this article highlight the effect of the conductive nanostructures as SWCNTs in the CNC films prepared by the EISA method but also the effect of the humidity conditions. SWCNT concentrations significantly affect the electrical conductivity of the films, and this behavior is dependent on the storage conditions of the nanohybrids. Furthermore, it was shown that SDS enables improved SWCNT dispersion in the system. The conductivity increase for the CNC nanohybrid film with SWCNT introduction and for the humidity conditions could be important phenomena that can find relevant applications in fields including sensing and energy storage.

ASSOCIATED CONTENT

Supporting Information

The Supporting Information is available free of charge at https://pubs.acs.org/doi/10.1021/acs.jpcc.0c03394.

FE-SEM micrographs of the fracture cross section and AC conductivity plots of nanohybrids (PDF)

AUTHOR INFORMATION

Corresponding Author

Ilaria Armentano − *Department of Economics, Engineering, Society and Business Organization (DEIM), University of Tuscia, Largo dell'Università snc, 01100 Viterbo, Italy;* orcid.org/0000-0002-8266-4366; Email: ilaria.armentano@unitus.it

Authors

Ainhoa Angulo Dehesa − *Department of Graphic Design and Engineering Projects, Faculty of Engineering in Bilbao, University of the Basque Country (UPV/EHU), Bilbao 48013, Spain; Civil and Environmental Engineering Department, UdR INSTM, University of Perugia, 05100 Terni, Italy*

Francesca Luzi − *Civil and Environmental Engineering Department, UdR INSTM, University of Perugia, 05100 Terni, Italy;* orcid.org/0000-0001-8785-5033

https://dx.doi.org/10.1021/acs.jpcc.0c03394
J. Phys. Chem. C 2020, 124, 14901−14910

Debora Puglia − *Civil and Environmental Engineering Department, UdR INSTM, University of Perugia, 05100 Terni, Italy;* orcid.org/0000-0001-8515-7813

Erlantz Lizundia − *Department of Graphic Design and Engineering Projects, Faculty of Engineering in Bilbao, University of the Basque Country (UPV/EHU), Bilbao 48013, Spain; BCMaterials, Basque Center for Materials, Applications and Nanostructures, 48940 Leioa, Spain;* orcid.org/0000-0003-4013-2721

Luigi Torre − *Civil and Environmental Engineering Department, UdR INSTM, University of Perugia, 05100 Terni, Italy;* orcid.org/0000-0001-7872-5712

Complete contact information is available at: https://pubs.acs.org/10.1021/acs.jpcc.0c03394

Author Contributions

A.A.D.: Investigation and methodology. F.L.: Investigation, methodology, and writing. D.P.: Data analysis and writing (original draft and review and editing). I.A.: Conceptualization, writing (original draft and review and editing), and formal analysis. L.T.: Project administration. E.L.: Formal analysis, investigation, methodology, writing (original draft and review and editing), and resources. All of the data used to support the findings of this study are included in the article.

Author Contributions

[⊥]A.A.D. and F.L. contributed equally to this work

Notes

The authors declare no competing financial interest.

■ ACKNOWLEDGMENTS

A.A.D. thanks GARAPEN (Basque Association of Development Agencies) for the Global Training grant. The authors acknowledge financial support from the Global Training program of the Basque Government.

■ REFERENCES

(1) Kafy, A.; Sadasivuni, K. K.; Kim, H. C.; Akther, A.; Kim, J. Designing flexible energy and memory storage materials using cellulose modified graphene oxide nanocomposites. *Phys. Chem. Chem. Phys.* **2015**, *17*, 5923−5931.

(2) Kim, J.; Yun, S. Discovery of cellulose as a smart material. *Macromolecules* **2006**, *39*, 4202−4206.

(3) Kim, J.; Mun, S.; Ko, H.; Yun, G. Disposable chemical sensors and biosensors made on cellulose paper. *Nanotechnology* **2014**, *25*, 092001.

(4) Dufresne, A. Nanocellulose: A new ageless bionanomaterial. *Mater. Today* **2013**, *16*, 220−227.

(5) Trache, D.; Hussin, M. H.; Haafiz, M. K. M.; Thakur, V. K. Recent progress in cellulose nanocrystals: sources and production. *Nanoscale* **2017**, *9*, 1763−86.

(6) Klemm, D.; Cranston, E. D.; Fischer, D.; Gama, M.; Kedzior, S. A.; Kralisch, D.; Kramer, F.; Kondo, T.; Lindstrom, T.; Nietzsche, S.; Petzold-Welcke, K.; Rauchfuß, F. Nanocellulose as a natural source for groundbreaking applications in materials science: Today's state. *Mater. Today* **2018**, *21*, 720−748.

(7) Lizundia, E.; Goikuria, U.; Vilas, J. L.; Cristofaro, F.; Bruni, G.; Fortunati, E.; Armentano, I.; Torre, L. Metal nanoparticles embedded in cellulose nanocrystal based films: material properties and post-use analysis. *Biomacromolecules* **2018**, *19*, 2618.

(8) Yang, J.; Zhang, E.; Li, X.; Zhang, Y.; Qu, J.; Yu, Z. Z. Cellulose/graphene aerogel supported phase change composites with high thermal conductivity and good shape stability for thermal energy storage. *Carbon* **2016**, *98*, 50−57.

(9) Koga, H.; Saito, T.; Kitaoka, T.; Nogi, M.; Suganuma, K.; Isogai, A. Transparent, Conductive, and Printable Composites Consisting of TEMPO-Oxidized Nanocellulose and Carbon Nanotube. *Biomacromolecules* **2013**, *14*, 1160−1165.

(10) Hamedi, M. M.; Hajian, A.; Fall, A. B.; Hkansson, K.; Salajkova, M.; Lundell, F.; Wgberg, L.; Berglund, L. A. Highly conducting, strong nanocomposites based on nanocellulose-assisted aqueous dispersions of single-wall carbon nanotubes. *ACS Nano* **2014**, *8*, 2467−2476.

(11) Meng, Q.; Manas-Zloczower, I. Carbon nanotubes enhanced cellulose nanocrystals films with tailorable electrical conductivity. *Compos. Sci. Technol.* **2015**, *120*, 1−8.

(12) Ebert, L. B. Science of fullerenes and carbon nanotubes. *Carbon* **1997**, *35*, 437−8.

(13) Iijima, S.; Ichihashi, T. Single-shell carbon nanotubes of 1-nm diameter. *Nature* **1993**, *363*, 603−5.

(14) Li, S.; Lee, P. S. Development and applications of transparent conductive nanocellulose paper. *Sci. Technol. Adv. Mater.* **2017**, *18*, 620−33.

(15) Lizundia, E.; Puglia, D.; Nguyen, T. D.; Armentano, I. Cellulose nanocrystal based multifunctional nanohybrids. *Prog. Mater. Sci.* **2020**, *112*, 100668.

(16) Li, Y. Y.; Wang, B.; Ma, M. G.; Wang, B. Review of recent development on preparation, properties, and applications of cellulose-based functional materials. *Int. J. Polym. Sci.* **2018**, *2018*, 8973643.

(17) Golmohammadi, H.; Morales-Narváez, E.; Naghdi, T.; Merkoçi, A. Nanocellulose in sensing and biosensing. *Chem. Mater.* **2017**, *29*, 5426−46.

(18) Kafy, A.; Akther, A.; Shishir, M. I. R.; Kim, H. C.; Yun, Y.; Kim, J. Cellulose nanocrystal/graphene oxide composite film as humidity sensor. *Sens. Actuators, A* **2016**, *247*, 221−6.

(19) Lizundia, E.; Maceiras, A.; Vilas, J. L.; Martins, P.; Lanceros-Mendez, S. Magnetic Cellulose Nanocrystal Nanocomposites for the Development of Green Functional Materials. *Carbohydr. Polym.* **2017**, *175*, 425−432.

(20) Jiang, M.; Seney, R.; Bayliss, P. C.; Kitchens, C. L. Carbon Nanotube and Cellulose Nanocrystal Hybrid Films. *Molecules* **2019**, *24* (14), 2662.

(21) Olivier, C.; Moreau, C.; Bertoncini, P.; Bizot, H.; Chaveut, O.; Cathala, B. Cellulose Nanocrystal-Assisted Dispersion of Luminescent Single-Walled Carbon Nanotubes for Layer-by-Layer Assembled Hybrid Thin Films. *Langmuir* **2012**, *28* (34), 12463−12471.

(22) Xu, J.; Nguyen, T.-D.; Xie, K.; Hamad, W. Y.; MacLachlan, M. J. Chiral Nematic Porous Germania and Germanium/carbon Films. *Nanoscale* **2015**, *7* (31), 13215−13223.

(23) Lizundia, E.; Nguyen, T.-D.; Vilas, J. L.; Hamad, W. Y.; Maclachlan, M. J. Chiroptical Luminescent Nanostructured Cellulose Films. *Mater. Chem. Front.* **2017**, *1* (1), 979−987.

(24) Beck, S.; Bouchard, S.; Berry, R. Dispersibility in Water of Dried Nanocrystalline Cellulose. *Biomacromolecules* **2012**, *13* (5), 1486−1494.

(25) Ratna, D.; Abraham, T. N.; Siengchin, S.; Karger-Kocsis, J. Novel Method for Dispersion of Multiwall Carbon Nanotubes in Poly(ethylene Oxide) Matrix Using Dicarboxylic Acid Salts. *J. Polym. Sci., Part B: Polym. Phys.* **2009**, *47* (12), 1156−1165.

(26) Meng, Q.; Manas-Zloczower, I. Carbon Nanotubes Enhanced Cellulose Nanocrystals Films with Tailorable Electrical Conductivity. *Compos. Sci. Technol.* **2015**, *120*, 1−8.

(27) Duan, W. H.; Wang, Q.; Collins, F. Dispersion of carbon nanotubes with SDS surfactants: a study from a binding energy perspective. *Chem. Sci.* **2011**, *2*, 1407−1413.

(28) Goikuria, U.; Larrañaga, A.; Vilas, J. L.; Lizundia, E. Thermal stability increase in metallic nanoparticles-loaded cellulose nanocrystal nanocomposites. *Carbohydr. Polym.* **2017**, *171*, 193−201.

(29) Nguyen, H. K.; Bae, J.; Hur, J.; Park, S. J.; Park, M. S.; Kim, I. T. Tailoring of Aqueous-Based Carbon Nanotube−Nanocellulose Films as Self-Standing Flexible Anodes for Lithium-Ion Storage. *Nanomaterials* **2019**, *9* (4), 655.

(30) Zhang, R.; Liu, Y. High energy oxidation and organosolvsolubilization for high yield isolation of cellulose nanocrystals (CNC) from Eucalyptus hardwood. *Sci. Rep.* **2018**, *8*, 16505.
(31) Sun, J.; Zhang, C.; Yuan, Z.; Ji, X.; Fu, Y.; Li, H.; Qin, M. Composite Films with Ordered Carbon Nanotubes and Cellulose Nanocrystals. *J. Phys. Chem. C* **2017**, *121* (16), 8976−8981.
(32) Maria, K. H.; Mieno, T. Production and Properties of Carbon Nanotube/Cellulose Composite Paper. *J. Nanomater.* **2017**, *2017*, 6745029.
(33) Corgié, S. S.; Smith, H. M.; Walker, L. P. Enzymatic transformations of cellulose assessed by quantitative high-throughput fourier transform infrared spectroscopy (QHT-FTIR. *Biotechnol. Bioeng.* **2011**, *108* (7), 1509−1520.
(34) Peng, H.; Reverdy, P.; Khabashesku, V. N.; Margrave, J. L. Sidewall functionalization of single-walled carbon nanotubes with organic peroxides. *Chem. Commun.* **2003**, *3*, 362−363.
(35) Hamad, W. Y.; Hu, T. Q. Structure-Process-Yield Interrelations in Nanocrystalline Cellulose Extraction. *Can. J. Chem. Eng.* **2010**, *88* (3), 392−402.
(36) Lin, N.; Bruzzese, C.; Dufresne, A. TEMPO-Oxidized Nanocellulose Participating as Crosslinking Aid for Alginate-Based Sponges. *ACS Appl. Mater. Interfaces* **2012**, *4* (9), 4948−4959.
(37) Yao, Q.; Wang, Q.; Wang, L.; Chen, L. Abnormally Enhanced Thermoelectric Transport Properties of SWNT/PANI Hybrid Films by the Strengthened PANI Molecular Ordering. *Energy Environ. Sci.* **2014**, *7* (11), 3801−3807.
(38) Smith, L. A.; Hammond, R. B.; Roberts, K. J.; Machin, D.; McLeod, G. Determination of the Crystal Structure of Anhydrous Sodium Dodecyl Sulphate Using a Combination of Synchrotron Radiation Powder Diffraction and Molecular Modelling Techniques. *J. Mol. Struct.* **2000**, *554* (2), 173−182.
(39) Wang, W.; Lu, H.; Liu, Y.; Leng, J. Sodium Dodecyl Sulfate/epoxy Composite: Water-Induced Shape Memory Effect and Its Mechanism. *J. Mater. Chem. A* **2014**, *2* (15), 5441−5449.
(40) Lizundia, E.; Sarasua, J. R.; D'Angelo, F.; Orlacchio, A.; Martino, S.; Kenny, J. M.; Armentano, I. Biocompatible Poly(L-lactide)/MWCNT Nanocomposites: Morphological Characterization, Electrical Properties, and Stem Cell Interaction. *Macromol. Biosci.* **2012**, *12* (7), 870−881.
(41) Monti, M.; Armentano, I.; Faiella, G.; Antonucci, V.; Kenny, J. M.; Torre, L.; Giordano, M. Toward the microstructure - properties relationship in MWCNT/epoxy composites: percolation behavior and dielectric spectroscopy. *Compos. Sci. Technol.* **2014**, *96*, 38−46.
(42) Logakis, E.; Pandis, Ch.; Peoglos, V.; Pissis, P.; Pionteck, J.; Potschke, P.; Micusik, M.; Omastova, M. Electrical/dielectric properties and conduction mechanism in melt processed polyamide/multi-walled carbon nanotubes composites. *Polymer* **2009**, *50*, 5103−5111.
(43) Dissado, L. Dielectric Response. In *Springer Handbook of Electronic and Photonic Materials*; Kasap, S., Capper, P., Eds.; Springer Handbooks: Cham, 2017.
(44) Le Bras, D.; Strømme, M.; Mihranyan, A. Characterization of Dielectric Properties of Nanocellulose from Wood and Algae for Electrical Insulator Applications. *J. Phys. Chem. B* **2015**, *119*, 5911−5917.
(45) Lindman, B.; Medronho, B.; Alves, A.; Costa, C.; Edlund, H.; Norgren, M. The relevance of structural features of cellulose and its interactions to dissolution, regeneration, gelation and plasticization phenomena. *Phys. Chem. Chem. Phys.* **2017**, *19*, 23704−23718.
(46) Mougel, J. B.; Bertoncini, P.; Cathala, B.; Chauvet, O.; Capron, I. Macroporous hybrid Pickering foams based on carbon nanotubes and cellulose nanocrystals. *J. Colloid Interface Sci.* **2019**, *544*, 78−87.
(47) Xu, D.; Sridhar, V.; Mahapatra, S. P.; Kim, J. K. Dielectric properties of exfoliated graphite reinforced flouroelastomer composites. *J. Appl. Polym. Sci.* **2009**, *111*, 1358−68.
(48) Fatemi, S. M.; Foroutan, M. Recent developments concerning the dispersion of carbon nanotubes in surfactant/polymer systems by MD simulation. *Journal of Nanostructure in Chemistry* **2016**, *6*, 29−40.
(49) Tan, Z.; Xu, H.; Abe, H.; Naito, M.; Ohara, S. Anisotropic polyhedral self-assembly of Ag-CNT nanocomposites. *J. Nanosci. Nanotechnol.* **2010**, *10*, 3978−3982.
(50) Valmalette, J.; Tan, Z.; Abe, H.; Ohara, S. Raman scattering of linear chains of strongly coupled Ag nanoparticles on SWCNTs. *Sci. Rep.* **2015**, *4*, 5238.

https://dx.doi.org/10.1021/acs.jpcc.0c03394
J. Phys. Chem. C 2020, 124, 14901−14910